Experimentally Consistent Ion Association Predicted for Metal Solutions from Free Energy Simulations

Richard P. Matthews and Kevin J. Naidoo*

Scientific Computing Research Unit, University of Cape Town, Rondebosch 7701, South Africa, and Department of Chemistry, University of Cape Town, Rondebosch 7701, South Africa

Received: December 14, 2009; Revised Manuscript Received: March 15, 2010

The calculation of association constants from computer simulations has historically been complicated because of difficulties in validating metal ion force fields for solution simulations. Here we develop a method that produces a force field for divalent metal ions in metal sulfate solutions (i.e., $Mg^{2+}SO_4^{2-}$, $Ca^{2+}SO_4^{2-}$, $Mn^{2+}SO_4^{2-}$, $Fe^{2+}SO_4^{2-}$, $Co^{2+}SO_4^{2-}$, $Ni^{2+}SO_4^{2-}$, $Cu^{2+}SO_4^{2-}$, and $Zn^{2+}SO_4^{2-}$). Using free energy of perturbation calculations, we are able to calibrate the potential of mean force $W(r)$ for these metal sulfate solutions. The calibrated free energy profiles then allow us to produce association constants for contact, solvent-shared, and solvent-separated ion pairs that are in excellent agreement with available ultrasonic and dielectric spectroscopic data. This metal solution force field is accurate for the calculation of relative free energies from physical and biophysical computer simulations.

1. Introduction

Ions and their formation salts play an integral part in several biological processes, where they behave as either active participants, cofactors, or salt buffers. Divalent metal ions such as the alkaline earth metals (Mg and Ca) and the divalent transition metals (Fe, Cu, Mn, and Zn) have been shown to play extensive roles in aiding the structural stability of proteins, and in the regulation of enzymatic reactions, in which they act as metal cores for metalloproteins and metalloenzymes.[1−3] Metal ions such as Ca play important roles in activating brain enzymes by flowing through ion channels signaling enzyme activation via complexation with calmodulin and through EF-hand motifs,[1,4] in the contraction of muscles via Ca-induced conformational change, and in mammalian fertilization.[5] Furthermore, Mg is a common cofactor used in the synthesis, repair, and modification of RNA and DNA,[6] while Zn and Fe play central roles in the development of Alzheimer's and Parkinson's diseases.[7] In chemistry, ion association affects chemical reaction rates, ion-exchange mechanisms, and solvent extraction. The latter is widely used in hydrometallurgical processes of which platinum group metal (PGM) extraction and transport[8] as well as base metal extraction are commercially important examples.[9] In both chemical and biological processes, the metal ions investigated here are generally hydrated[3,10] and may associate with hydrated ions with the opposite charge to form ion pairs.[11,12] The extent of ion pair formation in electrolyte solutions is generally low, but it occurs more frequently with an increase in salt concentration,[12] with increases in solvent temperature,[13,14] and via the use of solvents with low dielectric constants.[12,15]

Metal sulfate ion pairs in 2:2 electrolyte solutions have been under investigation for several decades using a multitude of experimental techniques.[13,14,16,17] However, limited computational studies have been conducted.[2,18,19] The majority of these studies have adopted the Eigen and Tamm three-step association mechanism based on their results for $MgSO_4$. They proposed that strongly hydrated ions associate via a three-step process in which the initial free hydrated ions (C and A for cation and anion, respectively) initially form solvent-separated ion pairs (SSIP or 2SIP), followed by solvent-shared ion pairs (SSHIP or SIP), followed by contact ion pairs (CIP). This process is believed to proceed via a stepwise release of several water molecules around the respective ions in steps 1 and 2 (outer-sphere coordination), terminating in step 3 in the formation of a complex (inner-sphere complexation) via ligand exchange,[20] as shown in Figure 1.

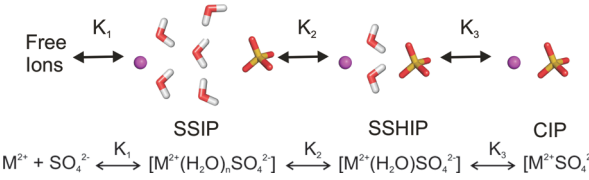

Figure 1. Ion pairing mechanism for divalent metal sulfate ions.

A convincing measure of the accuracy of computer simulations is the case when experimental observables are matched without the introduction of correction parameters. In the case of ion solutions, experiments have produced association constants for several divalent metal sulfate systems such as $MgSO_4$, $MnSO_4$, $CoSO_4$, $NiSO_4$, and $CuSO_4$. However, there have been difficulties in measuring the individual K_i association constants for several other species (e.g., $CaSO_4$ and $FeSO_4$), and only the overall K_a values have been obtained for all the metal sulfate systems. We are not aware of the calculation of association constants from molecular computer simulations for these divalent metal sulfate systems despite the critical importance of these properties. We believe that this is partly because the derivation of association constants from distribution functions or free energy profiles is complicated since these functions provide relative information about the CIP, SSHIP, and SIP configurations. In this work, we present a procedure for arriving at force field parameters for divalent metal sulfate (i.e., $Mg^{2+}SO_4^{2-}$, $Ca^{2+}SO_4^{2-}$, $Mn^{2+}SO_4^{2-}$, $Fe^{2+}SO_4^{2-}$, $Co^{2+}SO_4^{2-}$, $Ni^{2+}SO_4^{2-}$, $Cu^{2+}SO_4^{2-}$, and $Zn^{2+}SO_4^{2-}$) solution simulations that are of physical and biophysical importance. We calculate the association constants for $M^{2+}SO_4^{2-}$ ion pairing species from

* To whom correspondence should be addressed. E-mail: kevin.naidoo@uct.ac.za. Fax: +27-21-689-7499.

10.1021/jp911823x
Published on Web 05/12/2010

potential of mean force calculations. In doing so, we demonstrate that the force field and the method determining the association constants from free energy profiles are valid for solution simulations and reliable for the study of ion pairing in computer simulations.

2. Computational Methods

In all the aqueous solution simulations presented here, a TIP3P water model as implemented in CHARMM[21] is used. The sulfate ion used in all metal sulfate solutions was modeled using the literature potentials of Cannon et al. (sulfate and oxygen atom charges being +2.4 and −1.1, respectively, and Lennard-Jones parameters being $R_{min} = 1.99237$ and $\varepsilon = 0.25$ for S and $R_{min} = 1.76788$ and $\varepsilon = 0.25$ for O).[22] The metal Mg^{2+} ion was modeled using three previously published and commonly used parameter sets and one developed here. The published parameters were taken from (1) the CHARMM27 protein force field,[21] (2) the Aqvist force field,[23] and (3) the force field recently developed by Babu and Lim.[24] Ab initio calculations were performed using Gaussian03.[25] Minimum interaction energies and geometries of hydrated $Mg^{2+}(H_2O)_n$ ion species ($n = 1-6$) were determined by optimizing the intermolecular distance at the MP2/6-311++G(3d,3p) level in the same orientations used for alkali ions by Lamoureux and Roux[26] (see Table S1 of the Supporting Information) and later by Joung and Cheatham.[27] Water molecules were constrained at the TIP3P internal geometry as was done in previous parametrizations.[28] In the development of CHARMM parameters, interaction energies were fitted against HF/6-31G(d) ab initio calculated energies; however, in this study, the MP2/6-311++G(3d,3p) level was chosen as this gave the best metal water interaction energies. Inclusion of the counterpoise correction accounted for the basis set superposition error.[29]

After 5 ns of NPT (constant pressure at 1 bar) molecular dynamics (MD) simulations of the cation, anion, and 1020 water molecules using the CHARMM program,[21,30] the cubic simulation box sides converged and equilibrated to 33.98 Å. These box dimensions were used to perform canonical ensemble NVT MD simulations, which were analyzed, and the results are shown here. Potential of mean force (PMF) simulations of the two ions and 1020 water molecules were equilibrated in the same way, resulting in equilibrated cubic boxes with sides 33.98 Å in length. Periodic boundary conditions were used in the MD and PMF simulations where equations of motion were integrated using the Velocity-Verlet2 (vv2) integrator with a time step of 1 fs,[31] and the temperature was maintained at 298.15 K using a method based on the Nose-Hoover thermostat with a τ of 0.1.[31] Electrostatic interactions were calculated using the particle-mesh Ewald (PME) method[32] with a 16.0 Å real space cutoff, while the Lennard-Jones interactions were truncated using an atom-based switching function applied between 14.0 and 16.0 Å.

Free energy perturbation (FEP) calculations were performed on single ions and contact ion pair (CIP) ions that were placed at the center of a 24.3 Å water sphere initially containing 1941 TIP3P water molecules. Overlapping waters within 2.5 Å of the ions were deleted, and a spherical boundary force consistent with a water density of 1.0 g/cm^3 was applied to the droplet surface. The Verlet integrator[33] with a time step of 1 fs was used, and the temperature was kept at 298.15 K using a Nose-Hoover thermostat. Cutoffs using an atom-based switching function between 14.00 and 16.00 Å, for both electrostatic and van der Waal interactions, were used.

The Lorentz−Berthelot[34] combining rules in which ε_{ij} values are based on the geometric mean of ε_i and ε_j and $R_{min,ij}$ values are based on the arithmetic mean of $R_{min,i}$ and $R_{min,j}$, as follows:

$$\varepsilon_{ij} = \sqrt{\varepsilon_i \varepsilon_j} \tag{1a}$$

$$R_{min,ij} = (R_{min,ii} + R_{min,ij})/2 = R_{min,i} + R_{min,j} \tag{1b}$$

The PMFs for metal and sulfate ions (i.e., $Mg^{2+}SO_4^{2-}$, $Ca^{2+}SO_4^{2-}$, $Mn^{2+}SO_4^{2-}$, $Fe^{2+}SO_4^{2-}$, $Co^{2+}SO_4^{2-}$, $Ni^{2+}SO_4^{2-}$, $Cu^{2+}SO_4^{2-}$, and $Zn^{2+}SO_4^{2-}$) were calculated using the FEARCF method.[35]

The FEARCF method is designed to calculate free energy surfaces in multiple dimensions from probability distributions and histograms of the reaction coordinates. The reaction coordinate space is a discretized n-dimensional grid in which the sampling frequency for a bin site is recorded for each simulation. The case of ion pair association is the simplest implementation requiring only a one-dimensional grid. The population of this grid represents a running tally of the probability density for the distance between the ions, derived from the history of simulations to that point. It is used as input for a cubic-spline interpolation from which the reaction coordinate biasing forces are calculated. These forces are applied to all atoms used in the reaction coordinate definition to bias the next simulation's reaction coordinate trajectory away from previously sample areas. In this case, we consider the center of mass for the sulfate anion, which is located on the sulfur atom, and the forces are applied to the sulfur and oxygen atoms that make up the sulfate anion. The entire reaction coordinate space is equally sampled when the biasing forces are derived from the true PMF. The forces are applied on Cartesian coordinates, and therefore, the PMF does not need logarithmic Jacobian corrections.[36]

We calculate the effect of the perturbing forces generated from the reaction biasing potential $U(\xi)$. The free energy of association between two ions requires only one independent reaction coordinate ($\xi = r$). Adding $U(\xi)$ to the unbiased Hamiltonian changes the system Hamiltonian H_0

$$H(\xi) = H_0 + U(\xi) \tag{2}$$

The biased Hamiltonian $H(\xi)$ is then used in the simulation instead of H_0 and so generates a biased probability distribution of sampled coordinates $P'(\xi)$. This $P'(\xi)$ can then be converted to an unbiased probability distribution by accounting for the biasing potential as follows:

$$P'(\xi) = CP(\xi) \exp\left[\frac{U(\xi)}{k_B T}\right] \tag{3}$$

where C is the normalization constant, k_B is Boltzmann's constant, and T is the temperature of the system. The PMF for a calculated unbiased probability distribution is then

$$W(\xi) = -k_B T \log P(\xi) \tag{4}$$

The force arising from the treatment of the molecules as effective rigid bodies ensures that during the simulation, the atoms within each molecule do not move apart and deform the molecules because of differing accelerations that arise from the biasing potential. Consequently, when the resultant acceleration for these molecules is calculated as a whole, the forces on the atoms are determined such that the atoms experience the same resultant acceleration. The translational force arises from

a reaction coordinate ($\xi = r$), which is defined as a distance between two points, P_1 (metal atom) and P_2 (center of mass sulfate ion). A positive force in this case should increase the distance, and a negative deceases it by applying equal but opposite forces to the points that define the molecules. The force arising from the biasing potential for the reaction coordinate $\xi_1 = |\hat{r}| = r$ (i.e., the distance between P_1 and P_2) is $F(r) = \nabla W|_r$, which results in accelerations $a_{P_1} = -F/M_{P_1}$ and $a_{P_2} = -F/M_{P_2}$ on each molecule or ion. Here M_{P_1} and M_{P_2} are the masses of the metal ion at P_1 and sulfate anion at P_2, respectively, and the vector $\hat{r}$ connects P_1 on molecule 1 and P_2 on molecule 2. The accelerations, a_{P_1} and a_{P_2}, are then spread equally among the atoms of sulfate anion and the metal atom, such that the kth atom of the sulfate at P_2 experiences a force

$$\mathbf{f}_k(\xi) = \frac{\mathbf{F}(\xi)}{M} m_k \tag{5}$$

where m_k is the mass of atom k. The Cartesian force arising from the derivative of the potential with respect to r is then applied to the atoms of the molecules as

$$\mathbf{f}^r_{1,k} = -\frac{\partial U}{\partial r}\frac{m_k}{\sum_{i=1}^{N_1} m_i}(-\hat{r}), \quad \mathbf{f}^r_{2,k} = -\frac{\partial U}{\partial r}\frac{m_k}{\sum_{i=1}^{N_2} m_i}(\hat{r}) \tag{6}$$

with $\mathbf{f}_{2,k}(\xi)$ being the force on atom k of the sulfate molecular ion and $\mathbf{f}_1(\xi)$ being the force on the metal ion atom.

The biasing forces were calculated from the iteratively developing reaction coordinate free energy profile. The initial free energy profile guess is zero and is successively adapted on the basis of the sampling histogram of the preceding biased simulations. PMF calculations were conducted by placing the metal ion at the center of a water box and the sulfate ion an arbitrary distance from the metal ion. Several short (0.8 ns) simultaneous simulations were conducted at 298.15 K to develop the profile. These were then increased to longer run times (3 ns) using bins 0.125 Å in length, with an ion separation distance of up to 16.0 Å. The iterations were continued until a sampling ratio of at least 1:30 was obtained for the lowest-energy to highest-energy regions. A more detailed description of the FEARCF method has been previously presented.[35,37]

3. Metal Ion Parametrization

Metal ions and their solution interactions are governed by the nonbonded terms within the CHARMM force field. This is generally of the form

$$U(\vec{\mathrm{R}}) = \sum_{\text{nonbonds}} \left\{ \varepsilon_{ij}\left[\left(\frac{R_{\min,ij}}{r_{ij}}\right)^{12} - 2\left(\frac{R_{\min,ij}}{r_{ij}}\right)^{6}\right] + \frac{q_i q_j}{4\pi\varepsilon_0 D r_{ij}} \right\} \tag{7}$$

and includes the Coulomb and Lennard-Jones (LJ) 6-12 terms. In these terms, ε is the LJ well depth, $R_{\min,ij}$ is the distance at the LJ minimum, q is the partial atomic charge, D is the effective dielectric constant, and r_{ij} is the distance between atoms i and j.

In the derivation of the M^{2+} parameters, we are not concerned with the Coulomb term, as the metal charge is fixed at +2.0 throughout all testing and simulations. This leaves only the Lennard-Jones 6-12 term requiring parametrization, which is achieved via adjustment of the interatomic dispersion−attraction and repulsive potentials, or ε_{ij} and $R_{\min,ij}$ for each pair of distinct atoms. In this work, relative LJ parameters for Mg^{2+} were initially approximated from the interaction energy and distance obtained from a monohydrated Mg^{2+} ion ($R = 1.94$ Å, energy = −77.5 kcal/mol) using the method proposed by Mackerell (and references therein).[28] Then via an iterative series of FEP calculations, the absolute free energy of hydration of Mg^{2+} were tuned to match the experimental value by adjusting the LJ parameters. The LJ parameters were optimized by running several simulations at an ε of 0.02 or 0.03 for an $r_{\min}$ range of 0.7−2.0 Å in increments of 0.05 Å. The values producing the closest fit to the experimental[38] $\Delta G_{\text{hydration}}$ value were refined and used as the final Mg^{2+} parameters. Ion−water cluster energies given in the Supporting Information (Table S1) were then used to check the accuracy of the final parameters.

SCHEME 1

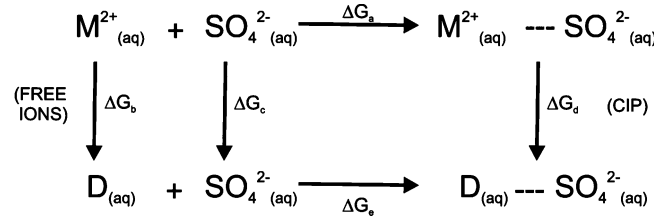

The solvated Mg^{2+} ion solution was minimized for 1000 steps using steepest descent, followed by equilibration for 100 ps at a mean temperature of 298.15 K. To calculate the hydration free energies of the ion, a two-stage perturbation approach was used. In the first stage, the charge of the ion was removed in water, and in the second stage, the van der Waals potentials were removed. Both charge removal and van der Waals potential removal were accomplished using 40 windows between the unperturbed ($\lambda = 0$) and perturbed ($\lambda = 1$) states, with each window being sampled for 100 ps. We iteratively performed the FEP simulations and adjusted the LJ parameters for the Mg^{2+} ion until we were able to produce a free energy of hydration of −437.4 kcal/mol which matched experimentally reported values.[38]

Next we calculated the free energy of association of a single Mg^{2+} and a single SO_4^{2-} ion, which we illustrate in Scheme 1. This was done by initially constraining the two ions (in vacuum) at a distance corresponding to the contact ion pair minima (as seen in the PMF profile). This CIP neutral species was placed at the center of a 24.3 Å water sphere, and the Mg^{2+} ion was perturbed to a dummy atom as described above, with the constraint still in place. Reverse perturbations were performed from configurations independent of the forward perturbation runs. The free energies for the forward and reverse runs were then averaged, and the free energy of hydration of the metal ion was subtracted from this to obtain the absolute free energy of the $MgSO_4$ electrolyte species.

The relative abundance of solution experimental data for Mg^{2+} and $MgSO_4$ presents this ion as an ideal candidate for benchmarking the parametrization of the divalent ion series. Consequently, this metal and the corresponding salt were used to calibrate all the divalent metal sulfates. Lennard-Jones parameters of the divalent metal ions Ca^{2+}, Mn^{2+}, Co^{2+}, Ni^{2+}, Cu^{2+}, and Zn^{2+} were derived from a series of FEP calculations in which these ions were perturbed from Mg^{2+} for the calculation of their free energies of hydration. The parametrization followed an iterative procedure in which the FEP calculations were repeated following an adjustment of the Lennard-Jones param-

TABLE 1: MSFF Parameter Set Shown with the Calculated Differences in Hydration Free Energies Relative to Mg^{2+} and the Corresponding Experimental Hydration Free Energies Taken from ref 38

ion	ε	$R_{min}/2$	ΔG_{expt}	$\Delta\Delta G_{expt}$	$\Delta\Delta G_{calcd}$
Mg^{2+}	0.020	1.0358	437.4	0.0	0.0
Ca^{2+}	0.030	1.521	359.7	77.7	77.7
Mn^{2+}	0.030	1.134	420.7	16.7	17.0
Fe^{2+}	0.030	0.983	439.8	−2.4	−2.3
Co^{2+}	0.030	0.798	457.7	−20.3	−19.8
Ni^{2+}	0.030	0.738	473.2	−35.8	−35.6
Cu^{2+}	0.030	0.762	480.4	−43.0	−41.8
Zn^{2+}	0.030	0.750	467.3	−29.9	−29.2

eters until the difference in free energies of hydration matched experimentally reported values.[38] These metal parameters will produce experimentally consistent results when using the TIP3P water model and may do so for other water models but has not been tested here. We now refer to this parameter set as the metal solution force field (MSFF) and list it along with its differences in free energies of hydration relative to Mg^{2+} in Table 1.

4. Calibrating Ion Association Free Energy Curves

The PMF has previously been used to determine ion pair species in dilute electrolyte solutions for NaCl under ambient[39] and supercritical conditions,[40,41] high-temperature aqueous H_3O^+/Cl^- solutions,[42,43] and a $Na^+/[PtCl_6]^{2-}$ system.[44,45] PMF calculations have also been used to determine ion pair thermodynamic properties for $CaSO_4$[18] and $(CH_3)_3CCl$.[46] As with structural data extracted from molecular dynamics simulations, PMF calculations are dependent on the parameters used in the simulation.[47] While ion association separation distances for CIP, SSHIP, and SIP ion pairs and the relative probability of occurrence for these ion pairs may be derived from the free energy curve, absolute free energies cannot be determined from a PMF profile without calibrating the curve.

The procedure of calibration is problematic, as unlike the interaction of a pair of neutral species, it cannot be assumed that at relatively large ion separations (i.e., >15 Å) the interaction between them is zero in the presence of the solvent. Therefore, setting the free energy of association to zero at a large distance such as one-half the simulation box length may not yield experimentally consistent values. Developing a reliable means of calibration is critical if PMFs are to be used to predict absolute solution properties such as overall and individual ion association equilibrium constants. Previously, Jorgensen calibrated PMFs using FEP calculations and from that derived absolute free energies for methane dimers.[48] However, while in that study the results were compared to predictions from the integral equation theory of Pratt and Chandler,[49] no solution observables such as association constants were calculated from the calibrated PMF.

The PMF could be adjusted by calculating its value at a specific point, $W(r_0)$, using the solvent dielectric constant, as proposed by Gaurdia[39] such that

$$W(r) = W(r_0 - k_B T) \ln P(r) \tag{8}$$

where k_B is Boltzmann's constant, T is the temperature, and $W(r_0)$ is a constant that should be suitably chosen to yield $W(r)$ values that are reliable at long separations. $W(r_0)$ may be computed from the Coulombic interaction energy at a selected distance[39,45]

$$W(r_0) = \frac{q_A q_C}{4\pi\kappa\varepsilon_0 r_0} \tag{9}$$

where q_A and q_C are the anion and cation charges, respectively, κ is the dielectric constant, ε_0 is the permittivity of free space, and r_0 is the selected anion−cation distance (in this work r_0 was selected to be 12 Å). This calculation is best conducted using the computational dielectric constant, κ_{comp}, corresponding to the solvent model employed in the simulation,[39] instead of the experimental dielectric, κ_{exp}. This is because the solvent model dielectric is not the same as that of the real solvent and the field experienced by the ion pair is that of the model solvent dielectric, not the true experimental field.[50] Calculating K_a values that match those measured in an experiment is an important measure of the accuracy of a simulation and the model used. Because the choice of κ has an exponential effect on computed K_a values, this method of calculating $W(r_0)$ is not reliable.

Using the MSFF, we calculate absolute free energies for the CIP of M^{2+} (M = Mg^{2+}, Ca^{2+}, Mn^{2+}, Fe^{2+}, Co^{2+}, Ni^{2+}, Cu^{2+}, and Zn^{2+}) and SO_4^{2-} from FEPs of the CIP as shown in Scheme 1 and by removing the contribution of the absolute free energy of hydration for each ion as listed in Table 1. These absolute free energies compare well with experimental values (Table 3) for the ion pairing hydration energies, although these have been measured for the combined individual CIP, SSHIP, and SIP species. Using these absolute free energy values at the CIP in the case of the MSFF, we will now show that adjusting the CIP PMF to that value results in effective calibration of the PMF.

5. Calculating K_a from PMF Profiles

In principle, association constants, K_a, can be calculated from radial distribution functions of anions (A) and cations (C), $g^{\infty}_{AC}(r)$, where at infinite dilution the relation is

$$K_a = 4\pi R \int_{r_0}^{r} g^{\infty}_{AC}(r) r^2 \, dr \tag{10}$$

and integration is performed over the region containing all ion pairing species and free ions. R is the conversion factor from cubic angstroms per molecule to cubic decimeters per mole (viz., R = 6.0221 × 10^{-4} dm^3 mol^{-1} $Å^{-3}$ $molecule^{-1}$). However, a direct

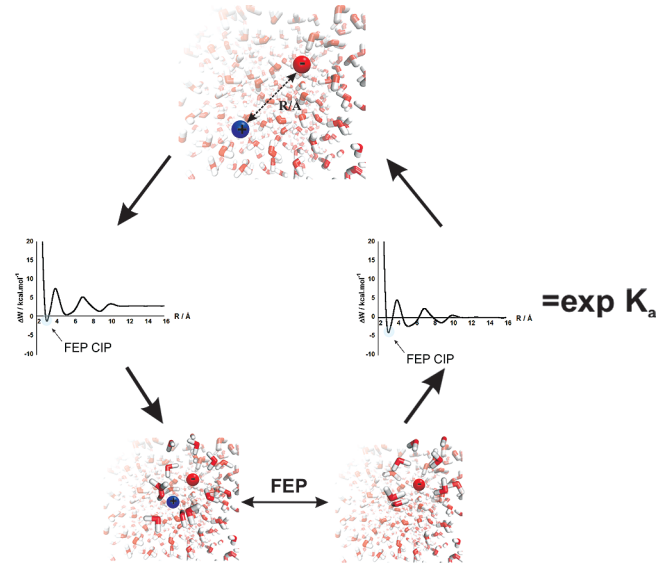

Figure 2. Summary of the method used to calibrate PMF profiles.

TABLE 2: Results from the Mg^{2+} Hydration FEP Cycle[a]

parameter set	ΔG_a	ΔG_b	ΔG_d
Aqvist	−3.35	−456.9	−453.55
Babu	−2.85	−451.7	−448.15
CHARMM	−1.28	−458.9	−457.62
MSFF	−1.19	−437.4	−436.21

[a] ΔG_a, ΔG_b, and ΔG_d are the free energies from the FEP cycle shown in Scheme 1.

determination of $g^{\infty}_{AC}(r)$ or an equivalent probability distribution function, $P(r)$, is computationally impractical because it involves infinite dilution and added to this the inability of conventional molecular dynamics simulations to sample high-energy barrier regions (greater than $3kT$) frequently, resulting in lengthy simulations.

Instead of this approach, the PMF in which the reaction coordinate is the distance r between the cation and anion can be used.[39,40,43,51] However, if $W(r_0)$ is computed correctly and included in the PMF, then K_a may be expressed in terms of $W(r)$ as

$$K_a = 4\pi R \int_{r_0}^{r} \exp\left[\frac{-W(r)}{k_B T}\right] r^2 \, dr \tag{11}$$

Here the value r in the definite integration is identical to that in eq 10, but the PMF curve has a maximum in this position, rather than the minimum in the $g^{\infty}_{AC}(r)$ curve. This representation leads to the calculation of the overall equilibrium constants of ion association. However, by choosing the integration limits that are specific for CIP, 2SIP, and SIP configurations, we can calculate the equilibrium rate constants (K_1, K_2, and K_3)[43]

$$K_1 = \frac{[\text{SSIP}]}{[\text{A}][\text{C}]} = \frac{\int_{r_2}^{r_3} \exp\left[\frac{-W(r)}{k_B T}\right] r^2 \, dr}{\int_{r_3}^{r_n} \exp\left[\frac{-W(r)}{k_B T}\right] r^2 \, dr} \tag{12a}$$

$$K_2 = \frac{[\text{SSHIP}]}{[\text{SSIP}]} = \frac{\int_{r_1}^{r_2} \exp\left[\frac{-W(r)}{k_B T}\right] r^2 \, dr}{\int_{r_2}^{r_3} \exp\left[\frac{-W(r)}{k_B T}\right] r^2 \, dr} \tag{12b}$$

$$K_3 = \frac{[\text{CIP}]}{[\text{SSHIP}]} = \frac{\int_{r_0}^{r_1} \exp\left[\frac{-W(r)}{k_B T}\right] r^2 \, dr}{\int_{r_1}^{r_2} \exp\left[\frac{-W(r)}{k_B T}\right] r^2 \, dr} \tag{12c}$$

In these equations, the individual ion pair species are integrated over specific regions; for example, the CIP is integrated from r_0 to r_1, where r_0 and r_1 are the positions of the first and second maxima of $W(r)$, respectively, or the boundaries of the free energy well corresponding to the CIP species.

TABLE 3: $M^{2+}SO_4^{2-}$ FEP Cycle Results for the MSFF Ion Parameters[a]

ion	ΔG_a	ΔG_b	ΔG_d
Mg^{2+}	−1.19	−437.40	−436.21
Ca^{2+}	−2.98	−359.70	−356.72
Mn^{2+}	−3.67	−420.40	−416.73
Fe^{2+}	−1.56	−439.70	−438.14
Co^{2+}	−2.76	−457.20	−454.44
Ni^{2+}	−1.80	−473.00	−471.20
Cu^{2+}	−1.79	−479.20	−477.42
Zn^{2+}	−0.56	−466.60	−466.04

[a] ΔG_a, ΔG_b, and ΔG_d are the free energies from the FEP cycle shown in Scheme 1.

TABLE 4: Association Constants Calculated from MSFF for $MgSO_4$ CIP, SSHIP, and SIP Configurations Using Different PMF Calibration Procedures

	K_a	K_1	K_2	K_3
one-half box length	199.03	86.1	1.28	0.03
Guardia correction	180.31	62.3	1.85	0.03
FEP calibration	167.64	56.36	1.94	0.02
experimental [13,14]	164.94	50.00	1.96	0.02

Here we show that the PMF may be calibrated using the absolute free energy of the CIP calculated from FEP as done in section 4. In Figure 2, we illustrate procedural steps for calibration of the $MgSO_4$ PMF using the absolute CIP value from FEP calculations. In Table 2, the absolute CIP values for $MgSO_4$ calculated from several metal parameter sets are listed, while in Table 3, the values calculated for the other metal sulfate systems are shown in comparison. The maximum favorable free energy (PMF local minima) CIP points on PMF curves were shifted to match the FEP calculated CIP free energy of

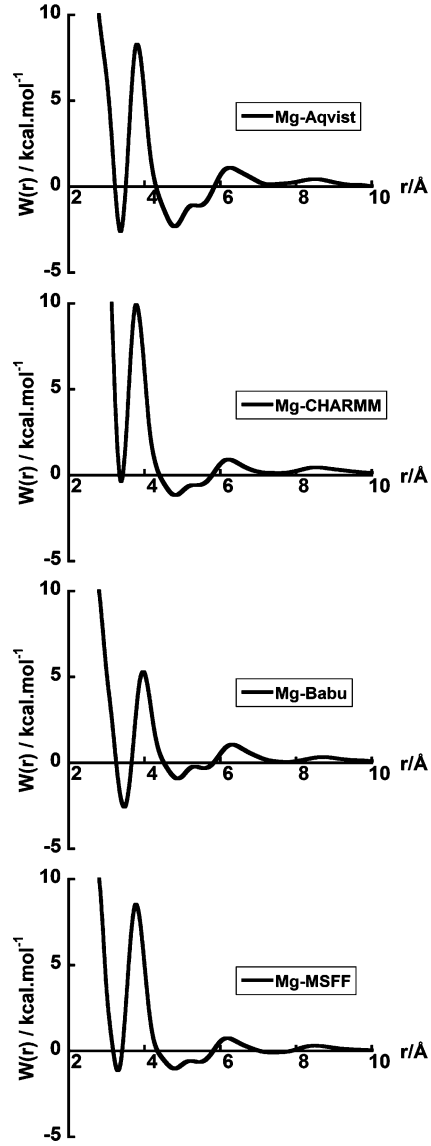

Figure 3. Comparison of FEP CIP-calibrated PMF profiles for $MgSO_4$ using several parameter sets.

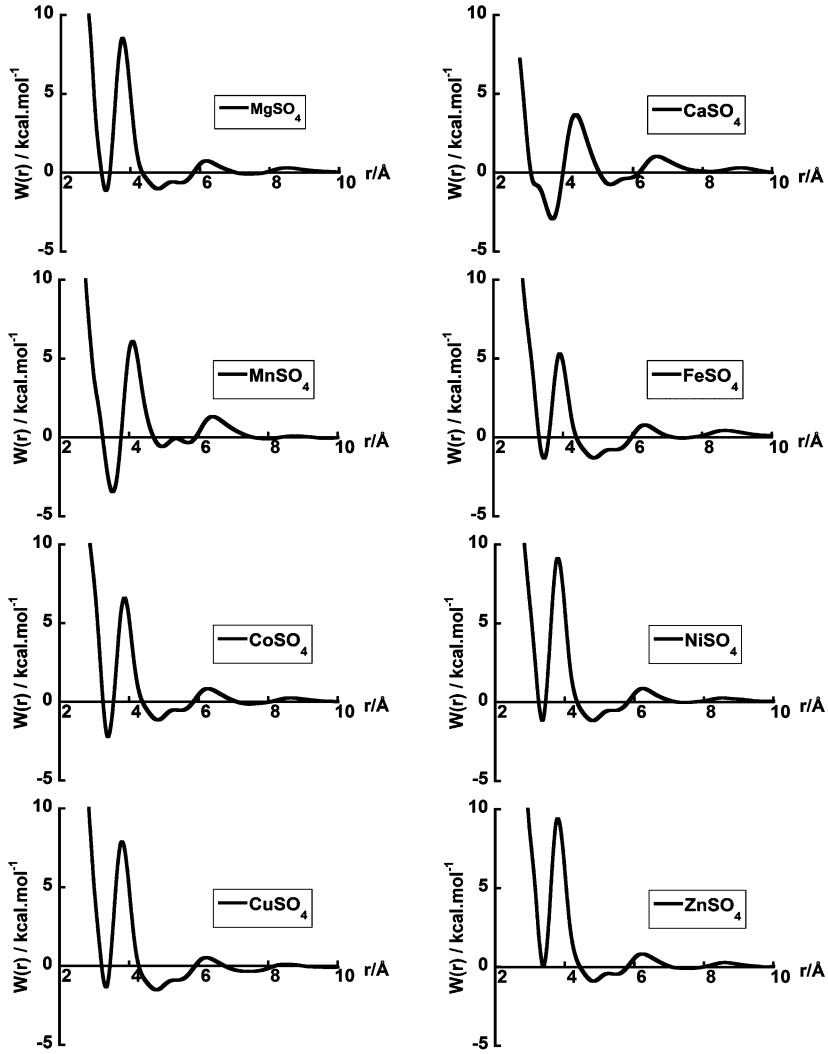

Figure 4. FEP CIP-calibrated PMF profiles of $M^{2+}SO_4^{2-}$ systems using the MSFF parameters.

association. Following this, the overall association constants and individual CIP, 2SIP, and SIP association constants were calculated for $Mg^{2+}SO_4^{2-}$.

Using $Mg^{2+}SO_4^{2-}$, we compare association constants calculated from the one-half box length, Guardia's $W(r_0)$, and the FEP CIP method of PMF calibration and report the results along with the experimentally measured values in Table 4. The one-half box length and the Gaurdia method both give an underestimation of 20% of the overall metal sulfate association constant, while the FEP method produces a K_a of 167.64 that is well within the accuracy of experimental error. The FEP CIP calibration is equally impressive in the reproduction of individual association constants as they compare perfectly with experimental values for SSIP ($K_1 = 56.36$), SSHIP ($K_2 = 1.94$), and CIP ($K_3 = 0.02$). The one-half box length and Guardia's method perform poorly; for example, K_1 is overestimated by 135 and 70% by each of these computational techniques, respectively.

The transferability of metal ion parameters is not often considered when solution properties or metal-containing proteins are being simulated.[52] Here we evaluate the performance of the MSFF parameters in relation to metal parameters currently used for ionic solution simulations. We compare the overall K_a values and individual association constants for each of the ion pair configurations (K_1, K_2, and K_3) produced from FEP CIP-calibrated PMFs using the Mg^{2+} parameters of Aqvist,[23] Babu and Lim,[24] CHARMM,[53] and MSFF in combination with the SO_4^{2-} anion parameters of Canon et al.[22] We used Lorentz−Berthelot combining rules for all the parameters, including those from the Aqvist force field, which we converted from geometric mean combining rules in the same way Cheatham[27] had done previously. The PMFs were calibrated using the specific FEP CIP absolute values produced for that force field (Figure 3). An analysis of the PMFs in Figure 4 reveals that all the PMFs show clearly defined CIP, SSHIP, and SSIP regions, with the CIP minima ranging from 3.375 to 3.750 Å for Mg to Ca. All the MSO_4 systems have a SSHIP broad region around 4−6 Å that is broken up into two minima (these minima correspond to different sulfate ion orientations relative to the metal centers). The SSIP regions are similarly broad, ranging from 7 to 10 Å, which reflects the increase in ion separation to the "free ion" configuration. The transition barrier from the SSHIP to CIP regions is significantly larger (i.e., 3−12 kcal/mol) compared with the barriers separating the other configurations. This is the energy required to remove a water layer between the ions resulting in a CIP. This energy increases with a decrease in the metal ion radius (i.e., an increased charge density). Furthermore, we observe that the CIP is favored over the SSHIP region, but as the charge density increases, this preference changes to the SSHIP being favored over the CIP. Finally, in the $CaSO_4$ PMF, an inflection point occurs within the CIP; this corresponds to the loss of a second water to form a bivalent CIP over the monovalent CIP. The $Mg^{2+}SO_4^{2-}$ association constants calcu-

TABLE 5: Comparison of Association Constants Calculated for $MgSO_4$ Using the FEP CIP PMF Calibration Method for Published Parameter Sets and the MSFF

	K_a	K_1	K_2	K_3
Aqvist	140.83	48.33	1.86	0.03
Babu	138.33	11.67	8.57	0.27
CHARMM	143.27	52.21	1.71	0.02
MSFF	167.64	56.36	1.94	0.02
experimental[14]	164.94	50.00	1.96	0.02

TABLE 6: Association Constants for $M^{2+}SO_4^{2-}$ Ion Pairs ($M = Mg^{2+}$, Ca^{2+}, Mn^{2+}, Fe^{2+}, Co^{2+}, Ni^{2+}, Cu^{2+}, and Zn^{2+}) Calculated from FEP CIP-Calibrated PMFs Using the MSFF Metal Ion Parameters Compared with Available Experimentally Measured Values

	simulation				experimental				
	K_a	K_1	K_2	K_3	K_a	K_1	K_2	K_3	ref
Mg^{2+}	167.64	56.36	1.94	0.02	164.94	50.00	1.96	0.02	17
Ca^{2+}	220.83	43.23	1.78	1.31	207.5	–	–	–	55
Mn^{2+}	165.81	53.41	0.45	3.21	139	52.63	0.37	3.52	56
Fe^{2+}	184.45	51.19	1.43	0.82	158	–	–	–	57
Co^{2+}	289.61	54.22	2.54	0.71	328	52.63	2.69	0.88	56[a]
Ni^{2+}	203.33	61.43	1.32	0.75	194.7	54.00	1.9	0.3	58
Cu^{2+}	183.36	58.21	1.72	0.25	190.8	54.00	1.95	0.3	14[a]
Zn^{2+}	201.77	51.27	1.96	0.49	199	–	–	–	13

[a] The values for Ni and Cu are not explicitly reported in the cited reference; we have calculated the values from the respective plots of K_i.

lated from the calibrated Aqvist, Babu and Lim, CHARMM, and MSFF PMFs are listed in Table 5. All the force fields other than the MSFF one underestimate K_a. The individual K_i ($i = 1$, 2, or 3) values produced from the Aqvist, Babu and Lim, and CHARMM force fields are not within the experimental error estimation, unlike the values produced from the MSFF.

A set of K_a values for the complete set of MSFF metal ion parameters that include the metal sulfates ($Ca^{2+}SO_4^{2-}$, $Mn^{2+}SO_4^{2-}$, $Fe^{2+}SO_4^{2-}$, $Co^{2+}SO_4^{2-}$, $Ni^{2+}SO_4^{2-}$, $Cu^{2+}SO_4^{2-}$, and $Zn^{2+}SO_4^{2-}$) are presented in Table 6. The CIP, followed by the SSHIP and then the SSIP, is favored in every system. All the ions (to varying degrees) show two minima within the SSHIP region separated by barriers with differing heights. These minima correspond to the reorientation (rotation and removal) of the waters between the ions, when the ions exchange between the SSIP and SSHIP regions. All the ions except Mn have a definitive SSIP region. The lack of a clearly defined SSIP region suggests that the $Mn^{2+}SO_4^{2-}$ ion configuration is governed by a two-step and not a three-step ion association mechanism. This observation is consistent with an earlier suggestion by Jackopin and Yeager.[54] The transition barrier going from the SSHIP to CIP ranges from ~4.5 to 11.1 kcal/mol for Ca to Mg, whereas the barrier going from CIP to SSHIP ranges from ~6.8 to 11.4 kcal/mol. Interestingly, there is little difference (0.4−2.2 kcal/mol) between the free energies of the SSHIP and CIP pairs.

6. Conclusions

We calculated van der Waals molecular mechanics parameters for a series of divalent metals commonly used in biological and materials aqueous solution simulations. The Mg^{2+} ion was used to benchmark the ion hydration free energy from a creation−annihilation FEP calculation in water. Using this value, we refined the magnesium Lennard-Jones parameters using the contact ion pair free energy value as a reference to the ultrasonically measured one. This allowed for the calculation of a parameter set for other divalent ions resulting in the MSFF. Using that parameter set along with FEP CIP PMF calibration method, we show that for $MgSO_4$, $MnSO_4$, $CoSO_4$, $NiSO_4$, and $CuSO_4$ the overall, CIP, SSHIP, and SIP association constants are in excellent agreement with experimentally measured ones. Moreover, we are able to predict the association constants for $CaSO_4$, $FeSO_4$, and $ZnSO_4$. The behavior of divalent metal ions is critically important in many physical and biophysical processes. The MSFF force field along with the FEP CIP PMF calibration method produces very accurate solution behavior, thus allowing the extent of the CIP, SSHIP, and SIP to be predicted using computer simulations. Although this is a relatively simple force field that does not include polarization and is pairwise additive, the degree of accuracy achieved may make the MSFF useful in the calculation of free energy differences in biophysical systems such as divalent metal-containing proteins.

Acknowledgment. This work is based upon research supported by the South African Research Chairs Initiative of the Department of Science and Technology and National Research Foundation to K.J.N. R.P.M. thanks Anglo American Platinum Corp. for doctoral fellowship support and the University of Cape Town for the K. W. Johnstone and Harry Crossley scholarships toward doctoral studies. We thank the CHPC for the use of their computer facilities for the FEP MD simulations. Finally, we thank referee 2 for carefully reading the manuscript and making helpful suggestions for its improvement.

Supporting Information Available: Differences in average binding energies for Mg-$n$$H_2O$ configurations from MM and ab initio calculations (Table S1). This material is available free of charge via the Internet at http://pubs.acs.org.

References and Notes

(1) Lippard, S. J. *Nat. Chem. Biol.* **2006**, *2*, 504.
(2) Zhuo, K. L.; Liu, H. X.; Zhang, X. K.; Liu, Y. H.; Wang, J. J. *Carbohydr. Res.* **2008**, *343*, 2428.
(3) Dudev, T.; Lim, C. *Annu. Rev. Biophys.* **2008**, *37*, 97.
(4) Lepsik, M.; Field, M. J. *J. Phys. Chem. B* **2007**, *111*, 10012.
(5) Berridge, M. J.; Bootman, M. D.; Lipp, P. *Nature* **1998**, *395*, 645.
(6) Bowen, L. M.; Dupureur, C. M. *Biochemistry* **2003**, *42*, 12643. Adhikari, S. *J. Biol. Chem.* **2006**, *281*, 29525.
(7) Barnham, K. J.; Bush, A. I. *Curr. Opin. Chem. Biol.* **2008**, *12*, 222.
(8) Bernardis, F. L.; Grant, R. A.; Sherrington, D. C. *React. Funct. Polym.* **2005**, *65*, 205. Bell, K. J.; Westra, A. N.; Warr, R. J.; Chartres, J.; Ellis, R.; Tong, C. C.; Blake, A. J.; Tasker, P. A.; Schroder, M. *Angew. Chem., Int. Ed.* **2008**, *47*, 1745.
(9) Youcef, M. H.; Benabdallah, T.; llikti, H.; Reffas, H. *Solvent Extr. Ion Exch.* **2008**, *26*, 534.
(10) Richens, D. T. *The Chemistry of Aqua Ions*; John Wiley & Sons Ltd.: Chichester, U.K., 2004.
(11) Riccardi, D.; Schaefer, P.; Yang, Yu. H.; Ghosh, N.; Prat-Resina, X.; Konig, P.; Li, G.; Xu, D.; Guo, H.; Elstner, M.; Cui, Q. *J. Phys. Chem. B* **2006**, *110*, 6458.
(12) Marcus, Y. *Ion Solvation*, 1st ed.; Wiley-Intersience: New York, 1985.
(13) Akilan, C.; Rohman, N.; Hefter, G.; Buchner, R. *ChemPhysChem* **2006**, *7*, 2319.
(14) Akilan, C.; Hefter, G.; Rohman, N.; Buchner, R. *J. Phys. Chem. B* **2006**, *110*, 14961.
(15) Moyer, B. A.; Bonnesen, P. V. Physical Factors in Anion Separations. In *Supramolecular Chemistry of Anions*; Bianchi, A., Bowman-James, K., Garcia-Espana, E., Eds.; Wiley-VCH: New York, 1997. The MSFF files in CHARMM format can be downloaded from http://scru.uct.ac.za/.
(16) Larson, J. W. *J. Phys. Chem.* **1970**, *74*, 3392. Buchner, R.; Chen, T.; Hefter, G. *J. Phys. Chem. B* **2004**, *108*, 2365. Eigen, M.; Tamm, K. Z. *Elektrochemie* **1962**, *66*, 93. Rudolph, W. W.; Irmer, G.; Hefter, G. T. *Phys. Chem. Chem. Phys.* **2003**, *5*, 5253. Pethybridge, A. D.; Taba, S. S. *J. Chem. Soc., Faraday Trans.* **1982**, *78*, 1331. Bester Rogac, M. *J. Chem. Eng. Data* **2008**, *53*, 1355. Bester Rogac, M.; Babic, V.; Perger, T. M.; Neueder, R.; Barthel, J. *J. Mol. Liq.* **2005**, *118*, 111. Hefter, G. *Pure Appl. Chem.* **2006**, *78*, 1571.

(17) Atkinson, G.; Petrucci, S. *J. Phys. Chem.* **1966**, *70*, 3122.
(18) Ghoufi, A.; Malfreyt, P. *Mol. Phys.* **2006**, *104*, 3787.
(19) Chaban, G. M.; Huo, W. M.; Lee, T. J. *J. Chem. Phys.* **2002**, *117*, 2532.
(20) Petrucci, S., Ed. *Ionic Interactions from Fused Solutions to Fused Salts, Volume 1: Equilibrium and Mass Transport*; Academic: New York, 1971; Vol. 1, pp 421.
(21) Brooks, B. R.; Brooks, C. L.; Mackerell, A. D.; Nilsson, L.; Petrella, R. J.; Roux, B.; Won, Y.; Archontis, G.; Bartels, C.; Boresch, S.; Caflisch, A.; Caves, L.; Cui, Q.; Dinner, A. R.; Feig, M.; Fischer, S.; Gao, J.; Hodoscek, M.; Im, W.; Kuczera, K.; Lazaridis, T.; Ma, J.; Ovchinnikov, V.; Paci, E.; Pastor, R. W.; Post, C. B.; Pu, J. Z.; Schaefer, M.; Tidor, B.; Venable, R. M.; Woodcock, H. L.; Wu, X.; Yang, W.; York, D. M.; Karplus, M. *J. Comput. Chem.* **2009**, *30*, 1545.
(22) Cannon, W. R.; Pettitt, B. M.; McCammon, J. A. *J. Phys. Chem.* **1994**, *98*, 6225. Mason, P. E.; Brady, J. W. *J. Phys. Chem. B* **2007**, *111*, 5669.
(23) Aqvist, J. *J. Phys. Chem.* **1990**, *94*, 8021.
(24) Babu, C. S.; Lim, C. *J. Phys. Chem. A* **2006**, *110*, 691.
(25) Frisch, M. J.; Trucks, G. W.; Schlegel, H. B.; Scuseria, G. E.; Robb, M. A.; Cheeseman, J. R.; Montgomery, J. A., Jr.; Vreven, T.; Kudin, K. N.; Burant, J. C.; Millam, J. M.; Iyengar, S. S.; Tomasi, J.; Barone, V.; Mennucci, B.; Cossi, M.; Scalmani, G.; Rega, N.; Petersson, G. A.; Nakatsuji, H.; Hada, M.; Ehara, M.; Toyota, K.; Fukuda, R.; Hasegawa, J.; Ishida, M.; Nakajima, T.; Honda, Y.; Kitao, O.; Nakai, H.; Klene, M.; Li, X.; Knox, J. E.; Hratchian, H. P.; Cross, J. B.; Bakken, V.; Adamo, C.; Jaramillo, J.; Gomperts, R.; Stratmann, R. E.; Yazyev, O.; Austin, A. J.; Cammi, R.; Pomelli, C.; Ochterski, J. W.; Ayala, P. Y.; Morokuma, K.; Voth, G. A.; Salvador, P.; Dannenberg, J. J.; Zakrzewski, V. G.; Dapprich, S.; Daniels, A. D.; Strain, M. C.; Farkas, O.; Malick, D. K.; Rabuck, A. D.; Raghavachari, K.; Foresman, J. B.; Ortiz, J. V.; Cui, Q.; Baboul, A. G.; Clifford, S.; Cioslowski, J.; Stefanov, B. B.; Liu, G.; Liashenko, A.; Piskorz, P.; Komaromi, I.; Martin, R. L.; Fox, D. J.; Keith, T.; Al-Laham, M. A.; Peng, C. Y.; Nanayakkara, A.; Challacombe, M.; Gill, P. M. W.; Johnson, B.; Chen, W.; Wong, M. W.; Gonzalez, C.; Pople, J. A. *Gaussian 03*, revision E.01; Gaussian, Inc.: Wallingford, CT, 2004.
(26) Lamoureux, G.; Roux, B. *J. Phys. Chem. B* **2006**, *110*, 3308.
(27) Joung, I. S.; Cheatham, T. E. *J. Phys. Chem. B* **2008**, *112*, 9020.
(28) Chen, I. J.; Yin, D. X.; MacKerell, A. D. *J. Comput. Chem.* **2002**, *23*, 199.
(29) Boys, S. F.; Bernardi, F. *Mol. Phys.* **1970**, *19*, 553.
(30) Brooks, B. R.; Bruccoleri, R. E.; Olafson, B. D.; States, D. J.; Swaminathan, S.; Karplus, M. *J. Comput. Chem.* **1983**, *4* (2), 187.
(31) Lamoureux, G.; Roux, B. *J. Chem. Phys.* **2003**, *119*, 3025.
(32) York, D. M.; Darden, T. A.; Pedersen, L. G. *J. Chem. Phys.* **1993**, *99*, 8345. Essmann, U.; Perera, L.; Berkowitz, M. L.; Darden, T.; Lee, H.; Pedersen, L. G. *J. Chem. Phys.* **1995**, *103*, 8577.
(33) Verlet, L. *Phys. Rev.* **1967**, *159*, 98.
(34) Allen, M. P.; Tildesley, D. J. *Computer Simulation of Liquids*, 1st ed.; Oxford Science Publications: Oxford, U.K., 1989.
(35) Strümpfer, J.; Naidoo, K. J. *J. Comput. Chem.* **2010**, *31*, 308.
(36) Berkowitz, M.; Karim, O. A.; McCammon, J. A.; Rossky, P. J. *Chem. Phys. Lett.* **1984**, *105*, 577. Belch, A. C.; Berkowitz, M.; McCammon, J. A. *J. Am. Chem. Soc.* **1986**, *108*, 1755. Trzesniak, D.; Kunz, A. P. E.; van Gunsteren, W. F. *ChemPhysChem* **2007**, *8*, 162. Khavrutskii, I. V.; Dzubiella, J.; McCammon, J. A. *J. Chem. Phys.* **2008**, *128*, 044106.
(37) Barnett, C. B.; Naidoo, K. J. *Mol. Phys.* **2009**, *107*, 1243.
(38) Marcus, Y. *Biophys. Chem.* **1994**, *51*, 111.
(39) Guardia, E.; Rey, R.; Padro, J. A. *Chem. Phys.* **1991**, *155*, 187.
(40) Chialvo, A. A.; Cummings, P. T.; Cochran, H. D.; Simonson, J. M.; Mesmer, R. E. *J. Chem. Phys.* **1995**, *103*, 9379.
(41) Gao, J.; Weiner, J. H. *Science* **1994**, *266*, 748.
(42) Chialvo, A. A.; Cummings, P. T.; Simonson, J. T. *J. Chem. Phys.* **2000**, *113*, 8093. Chialvo, A. A.; Ho, P. C.; Palmer, D. A.; Gruszkiewicz, M. S.; Cummings, P. T.; Simonson, J. M. *J. Phys. Chem. B* **2002**, *106*, 2047.
(43) Chialvo, A. A.; Cummings, P. T.; Simonson, J. T. *J. Mol. Liq.* **2003**, *103*−*104*, 235.
(44) Lienke, A.; Klatt, G.; Koch, K. R.; Robinson, D. J.; Naidoo, K. J. *Inorg. Chem.* **2001**, *40*, 2352. Naidoo, K. J.; Klatt, G.; Koch, K. R.; Robinson, D. J. *Inorg. Chem.* **2002**, *41*, 1845.
(45) Naidoo, K. J.; Lopis, A.; Westra, A. N.; Robinson, D. J.; Koch, K. R. *J. Am. Chem. Soc.* **2003**, *125*, 13330.
(46) Jorgensen, W. L.; Buckner, K.; Huston, S. E.; Rossky, P. J. *J. Am. Chem. Soc.* **1987**, *109*, 1891.
(47) Patra, M.; Karttunen, M. *J. Comput. Chem.* **2003**, *25*, 678. Gavryushov, S.; Linse, P. *J. Phys. Chem. B* **2006**, *110*, 10878.
(48) Jorgensen, W. L.; Buckner, J. K.; Boudon, S.; Tirado-Rives, J. *J. Chem. Phys.* **1988**, *89* (6), 3742.
(49) Pratt, L. R.; Chandler, D. *J. Chem. Phys.* **1977**, *67*, 3683. Jorgensen, W. L.; Ravimohan, C. *J. Chem. Phys.* **1985**, *83*, 3050. Jorgensen, W. L.; Buckner, J. K. *J. Phys. Chem.* **1987**, *91*, 6083.
(50) Wasserman, E.; Wood, B.; Brodholt, J. *Geochim. Acta* **1995**, 1. Höchtl, P.; Boresch, S.; Bitomsky, W.; Steinhauser, O. *J. Chem. Phys.* **1998**, *109*, 4927.
(51) Ciccotti, G.; Ferrario, M.; Hynes, J. T.; Kapral, R. *Chem. Phys.* **1989**, *129*, 241.
(52) Marrone, T. J.; Kenneth, M.; Merz, J. *J. Phys. Chem.* **1993**, *97*, 6524.
(53) MacKerell, A. D.; Bashford, D.; Bellott, M.; Dunbrack, R. L.; Evanseck, J. D.; Field, M. J.; Fischer, S.; Gao, J.; Guo, H.; Ha, S.; Joseph-McCarthy, D.; Kuchnir, L.; Kuczera, K.; Lau, F. T. K.; Mattos, C.; Michnick, S.; Ngo, T.; Nguyen, D. T.; Prodhom, B.; Reiher, W. E.; Roux, B.; Schlenkrich, M.; Smith, J. C.; Stote, R.; Straub, J.; Watanabe, M.; Wiorkiewicz-Kuczera, J.; Yin, D.; Karplus, M. *J. Phys. Chem. B.* **1998**, *102*, 3586.
(54) Jackopin, L. G.; Yeager, E. *J. Phys. Chem.* **1966**, *70*, 313.
(55) *CRC Handbook of Chemistry and Physics*, 61st ed.; CRC Press: Boca Raton, FL, 1974.
(56) Bhatti, S. S.; Lark, B. S. *Acustica* **1981**, *48*, 64.
(57) Izatt, R. M.; Eatough, D.; Christen, J.; Bartholo, Ch. *J. Chem. Soc. A* **1969**, 45. Izatt, R. M.; Eatough, D.; Christen, J.; Bartholo, Ch. *J. Chem. Soc. A* **1969**, 47.
(58) Chen, T.; Hefter, G.; Buchner, R. *J. Solution Chem.* **2005**, *34*, 1045.

JP911823X